PCCP

PAPER

View Article Online
View Journal | View Issue

Cite this: *Phys. Chem. Chem. Phys.*, 2015, **17**, 23384

Theoretical kinetic study for methyl levulinate: oxidation by OH and CH_3 radicals and further unimolecular decomposition pathways†

S. Thion,[ab] A. M. Zaras,*[a] M. Szőri*[c] and P. Dagaut[a]

Received 17th July 2015,
Accepted 13th August 2015

DOI: 10.1039/c5cp04194e

www.rsc.org/pccp

Biofuels may represent a promising alternative in terms of energy sustainability and emission control. Until recently, simple compounds including only a single specific functional group was in the focus of the biofuel research while reported data on more complex structures are scarcer. Presence of multiple functional groups can make molecules more attractive for oxidative species providing attacking site for fast oxidation. Including both a carbonyl and an ester group, methyl levulinate (ML) can be such an excellent biofuel candidate due to its cellulosic origin, although its combustion kinetics is still unresolved. This work reports the first computational kinetic study on methyl levulinate oxidation relevant to combustion conditions. Absolute rate constants for H-abstraction reactions by OH and CH_3 radicals were calculated using the G3//MP2/aug-cc-pVDZ level of theory coupled with Transition State Theory (TST). The fate of the forming ML radicals was also investigated by computing absolute rate constants for β-scission as well as for H-transfer reactions. The outcomes of this work show that the sites between the two functional groups are the most favorable for H-abstraction reactions, and that methyl vinyl ketone (MVK) and methyl acrylate (MAC) are expected to be the main intermediate products of methyl levulinate oxidation. The present results will be useful for further detailed kinetic modeling.

Introduction

Petroleum is the main raw material for various applications in chemistry including the production of transportation fuels which is the most important in terms of consumed quantities.[1] Fuel combustion is also a major source of pollutants and greenhouse gases such as carbon dioxide. These concerns as well as issues regarding petroleum's non-renewable nature highlight the need to reduce the dependence on fossil resources by finding sustainable alternative fuels or additives and to understand their oxidation. "Green Chemistry" is an alternative to petroleum based chemistry and has caught the interest of the scientific community for the last decades, with emphasis on the production of various chemicals from biomass. The development of methods to process biomass components *i.e.* cellulose, hemicellulose, and lignin to chemical platforms with a focus on yields, cost, and possibility for adaptation to industrial scale is a challenging task that receives growing attention.[2–4] Among these platforms one finds, furfural and levulinic acid[2,5,6] part of the ten most interesting compounds that can be produced from biomass, according to the US Department of Energy.[7] These versatile compounds can indeed be used as building blocks in various fields of applications such as polymers, solvents, or fuels production.[8] Alkyl levulinates are oxygenated species including both a keto and an ester group that can be produced from these two platforms. A large set of studies is available in the literature for the optimization of different strategies to synthesize these compounds.[9] Generally reported methods start with hemicellulose and cellulose conversion to xylose and glucose, respectively through hydrolysis. Another step then leads to furfural and 5-hydroxymethylfurfural which are intermediates for the formation of levulinic acid. Esterification is then required to obtain alkyl levulinates and is optimized by using different kinds of catalysts. Other processes starting directly from cellulose, hemicellulose, or furfuryl alcohol have also been reported.[9]

One of the possible applications for this family of compounds is their use as fuel additives for gasoline, diesel fuel, biodiesel or even blends, as described in the patent literature.[10–17] The main outcomes reported so far are potential decrease in terms of emissions (soot or NO_x), better lubricity or octane number enhancement for gasoline. Some fundamental studies

[a] *CNRS-ICARE, Institut de Combustion, Aérothermique, Réactivité et Environnement 1C, Avenue de la recherche scientifique, 45071 Orléans cedex 2, France. E-mail: aristotelis.zaras@cnrs-orleans.fr*
[b] *Université d'Orléans, 6 Avenue du Parc Floral, 45100 Orléans, France*
[c] *Department of Chemical Informatics, Faculty of Education, University of Szeged, Boldogasszony sgt. 6, Szeged, 6725, Hungary. E-mail: milan@jgypk.u-szeged.hu*

† Electronic supplementary information (ESI) available: Optimized geometries and vibrational frequencies of reactants and transition states as calculated at the MP2/aug-cc-pVDZ level of theory. See DOI: 10.1039/c5cp04194e

can be found in the conventional literature as well, with emphasis on ethyl and butyl levulinate. Christensen *et al.*[18] investigated the performance of a diesel/alkyl levulinate blend in a Cummins ISB engine and observed a decrease of soot formation, and an increase of lubricity and thermal conductivity. A biodiesel was also added to improve the blending at low temperature. Same kinds of observations were made by Janssen *et al.*,[19] but the emissions in terms of unburned hydrocarbons and CO levels were also found to be higher than with regular fuel, which highlights the need for optimization to overcome this issue. These works highlighted the potential of the alkyl levulinate class of compounds, but more fundamental studies are necessary in order to better understand the oxidation of these biofuels including their oxidation mechanisms and corresponding rate constants. This is even more important for such fuel additive having multiple oxygen containing functional groups in vicinity, since use of group additivity approximations to estimate rate coefficients results large error in the modelling of their oxidation mechanisms.

In this work, we studied the kinetics of oxidation of methyl levulinate (ML). *Ab initio* calculations in conjunction with Transition State Theory were used to compute rate constants for H atom-abstraction reactions from the fuel by OH and CH_3 radicals. To the authors' knowledge, this is the first theoretical study on methyl levulinate oxidation kinetics.

Computational methodology

The initial geometry of methyl levulinate was determined by systematic conformational search of MOE 2009.1 program.[20] Then all the electronic structure calculations were performed with the Gaussian 09 program suite.[21] Besides the hegemony of B3LYP functional in geometry optimization in theoretical kinetics, dysfunction of this popular functional has been reported several times[22,23] and it was also the case for the dimethyl ether + OH system[24] analogous to methyl levulinate. Therefore, geometry optimization and vibrational frequency calculations were conducted at the MP2[25]/aug-cc-pVDZ[26] level of theory. For the single-point energy calculations which were subsequently applied on the optimized structures the sequence of single-point energy calculations of G3B3 theory[27] was manually applied. G3 theory consists of single-point energy calculations at four higher levels of theory namely QCISD(T)/6-31G(d), MP4/6-31+G(d), MP4/6-31G(2df,p), and ultimately MP2/G3Large. As it was proved earlier, G3 theory can produce accurate energetic results for various properties including formation enthalpies.[28]

Each structure determined in this study was treated using the rigid rotor-harmonic oscillator approximation whereas the harmonic frequencies were scaled by a factor of 0.959 adopted from CCCBDB database.[29] Since the transition states were located, a vibrational analysis was conducted to ensure that each transition state structure demonstrates a single imaginary frequency which corresponds to the proper mode of vibration. First of all the vibrational modes of the reaction coordinate in the transition state structures were visually inspected using the GaussView[30] software and then intrinsic reaction coordinate (IRC) calculations were performed at the MP2/aug-cc-pVDZ level of theory, to ensure that the located transition states correspond to the proper reactants and products. Each IRC calculation involved between 150 and 200 steps at both reverse and forward reaction path direction, with step intervals of 0.06 a.u. Once the transition states were verified, Transition State Theory was applied in order to compute the rate coefficients ($k^{\mathrm{TST}}(T)$) by using the KiSThelP[31] program:

$$k^{\mathrm{TST}}(T) = \sigma \frac{k_{\mathrm{B}}T}{h}\left(\frac{RT}{P^0}\right)^{\Delta n} \mathrm{e}^{-\frac{\Delta^{\ddagger}G^0(T)}{k_{\mathrm{B}}T}},$$

where σ is the reaction path degeneracy, k_{B} is Boltzmann's constant, T is temperature, h is Planck's constant, $\Delta^{\ddagger}G^0(T)$ represents the standard Gibbs free energy of activation for the considered reaction and Δn = 1 or 0 for gas-phase bimolecular or unimolecular reactions, respectively. The obtained rate coefficients refer to the temperature range 500 to 1300 K and pressure (P^0) of 1 atm; the modified Arrhenius expressions ($k(T) = A(T/K)^n \mathrm{e}^{Ea/RT}$) are given for each reaction as results of the fits to the calculated rate constants ($k^{\mathrm{TST}}(T)$). All species were assumed to be in the electronic ground state except OH, for which the electronic partition function was calculated with a spin orbit splitting of 139.7 cm^{-1}.[32]

Furthermore the standard enthalpies of formation of the methyl-levulinate and its radicals were obtained using different composite models (CBS-QB3, G3B3 and G3//MP2/aug-cc-pVDZ) by atomization scheme as well as from two isomerization reactions in order to demonstrate the level of theory was appropriate.

Results and discussion

In order to characterize the thermodynamic properties of methyl levulinate important for combustion, the standard enthalpy of formation of the most stable conformer of methyl levulinate (see Fig. 1) has been determined.

The standard enthalpy of formation ($\Delta_{\mathrm{f}}H^0_{298.15\mathrm{K}}$) was calculated with CBS-QB3[33] through the atomization scheme, with and without Pitzer–Gwinn approximation of the hindered rotor. The obtained standard enthalpy of formation values of −141.9 and −143.0 kcal mol^{-1} respectively, reveal a very good agreement between the two different treatments.

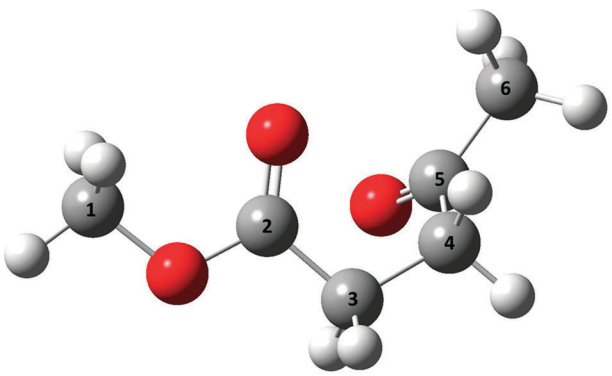

Fig. 1 Optimized structure of methyl levulinate.

Table 1 Calculated standard enthalpies of formation for methyl levulinate (1 kcal = 4.1868 kJ)

Methodology	Level of theory	$\Delta_f H^0_{298K}$ (kcal mol^{-1})
Atomization scheme	G3//MP2/aug-cc-pVDZ	−143.4
	G3B3	−143.5
	CBS-QB3	−143.0
Reaction (i)	G3//MP2/aug-cc-pVDZ	−142.9
	G3B3	−142.8
	CBS-QB3	−142.8
Reaction (ii)	G3//MP2/aug-cc-pVDZ	−141.6
	G3B3	−141.5
	CBS-QB3	−141.4

This implementation does not result into considerable improvement and therefore was neglected thereafter. In order to check the consistency of the result obtained for ML with the literature values of its isomers, two isomerization, isodesmic as well as isogyric, reactions (i and ii) were chosen, with respect to existing experimental enthalpies of formation.[34,35] Table 1 summarizes the calculated standard enthalpies of formation ($\Delta_f H^0_{298.15K}$) for methyl levulinate.

(i) Propanoic anhydride → Methyl levulinate

(ii) Ethyl acetoacetate → Methyl levulinate

Table 1 outlines two major outcomes. First that the G3//MP2/aug-cc-pVDZ level of theory which was chosen for the calculations throughout this work is in excellent agreement with the other two composite methods, regardless the methodology used (atomization scheme/isodesmic reaction). Second, that overall the obtained values of standard enthalpy of formation are highly consistent. These outcomes are promising regarding the accuracy of the results presented here. Based on these calculations the proposed enthalpy of formation for methyl levulinate (−142.5 ± 0.8 kcal mol^{-1}) is the average of the calculated values given in Table 1 and this is used for evaluating the heat of combustion value (HHV) as well (663.4 ± 0.8 kcal mol^{-1}). Furthermore, other thermodynamical properties such as the values of entropy (113.1 cal mol^{-1} K^{-1}) and constant pressure heat capacity (41.9 cal mol^{-1} K^{-1}) were also estimated based on CBS-QB3 calculations including hindered internal rotor treatment carried out by the CanTherm[36] software.

After discussion of the thermodynamic properties of the methyl levulinate, its different decomposition pathways studied are presented in Fig. 2. In our scheme, the initial oxidation occurs *via* bimolecular hydrogen abstraction reactions initiated by OH and CH_3 radicals. At combustion condition, the OH radical is expected to dominate these abstraction reactions, while the methyl radical reactions have been taken into consideration in an attempt to improve further the estimated kinetics of these reactions. Thereafter unimolecular decomposition pathways of the produced ML radicals (MLR) were also considered.

(a) Hydrogen abstraction reactions

Table 2 presents the total bimolecular rate constants for hydrogen abstraction by hydroxyl and methyl radicals,

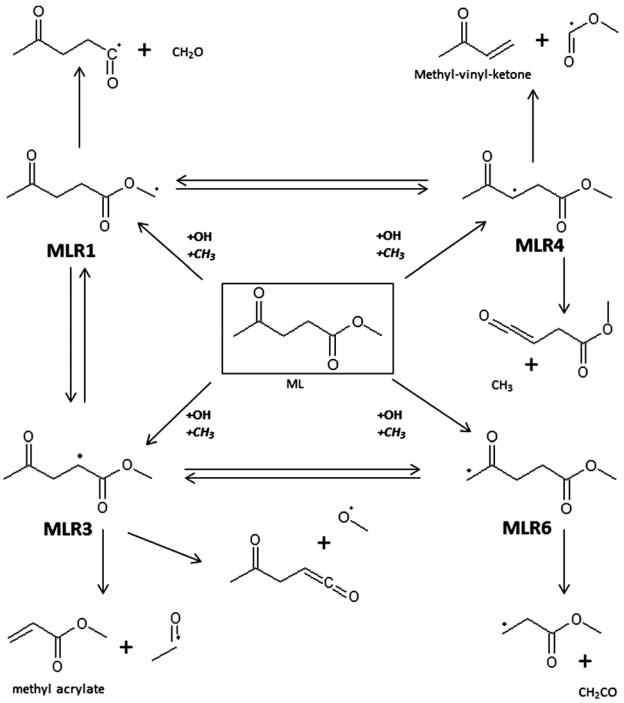

Fig. 2 Decomposition pathways of methyl levulinate considered in this work.

Table 2 Total hydrogen abstraction rate constants for methyl levulinate (ML). (Bold values: R = OH•, italic values: R = CH_3)

Reaction	A (cm^3 mol^{-1} s^{-1})	n	E_a (kcal mol^{-1})
ML + R• → MLR1 + RH	**3.50 × 10^0**	**3.79**	**−1.77**
	5.34 × 10^2	*3.22*	*11.05*
ML + R• → MLR3 + RH	**2.87 × 10^2**	**3.06**	**−2.32**
	5.46 × 10^1	*3.13*	*8.68*
ML + R• → MLR4 + RH	**3.25 × 10^3**	**2.89**	**−1.50**
	1.41 × 10^1	*3.29*	*8.33*
ML + R• → MLR6 + RH	**4.06 × 10^3**	**2.84**	**0.065**
	3.71 × 10^1	*3.12*	*9.98*

respectively. The notations of the produced radicals (MLRN, where N can be 1, 3, 4 and 6) refer to the scheme presented in Fig. 2. The total bimolecular rate constants were calculated as the sum of all the different transition states located at the same carbon site. In the rare cases that only one transition state was located and attributed to a particular carbon site, the total rate constant was determined as the multiple of the unique rate constant obtained and the number of the available hydrogen atoms in that particular site. Unsurprisingly, the bimolecular reactions involving the hydroxyl radical are significantly faster than the correspondingly methyl radical reactions, as they involve considerably smaller barriers.

Considering the OH reactions, the formation of 1-methoxy-1,4-dioxopentan-3-yl radical (MLR4) is the dominant channel over the entire temperature range studied here; it is followed by the 1-methoxy-1,4-dioxopentan-2-yl (MLR3) formation

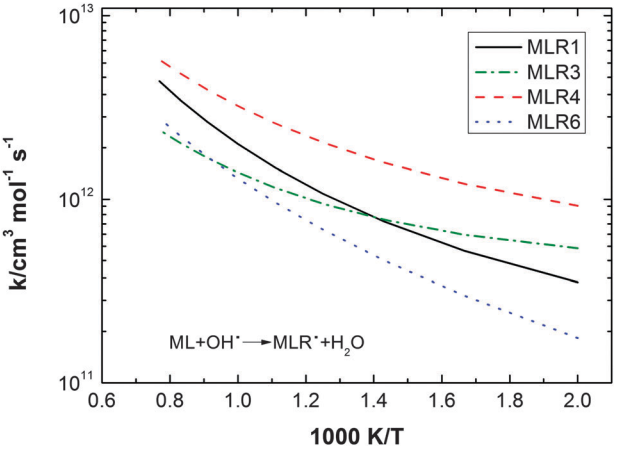

Fig. 3 Hydrogen abstraction rate constants for methyl levulinate (ML) with OH.

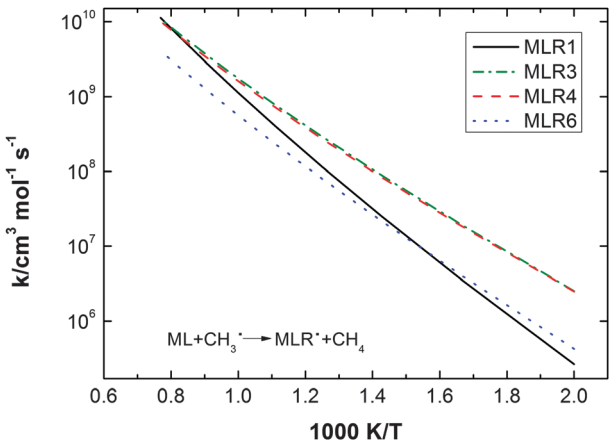

Fig. 4 Hydrogen abstraction rate constants for methyl levulinate (ML) with CH_3.

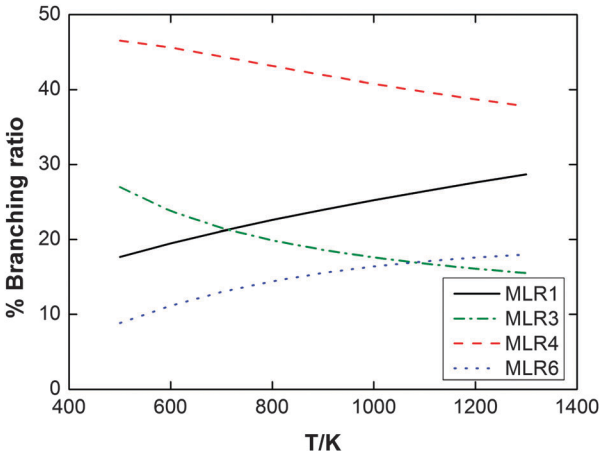

Fig. 5 Temperature dependent branching ratio for hydrogen abstraction reactions of methyl levulinate (ML) and OH.

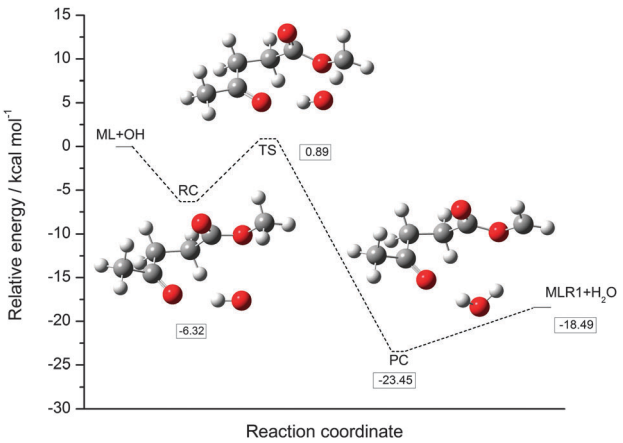

Fig. 6 Relative zero-point corrected potential energy diagram for the reaction ML + OH yielding MLR1 obtained from G3//MP2/aug-cc-pVDZ calculations. RC: pre-reaction complex, TS: transition state, PC: post-reaction complex.

below 714 K. Due to channel switching, the formation of ((4-oxopentanoyl)oxy)methyl radical (MLR1) became significant channel above 714 K. In the case of the H-abstraction by methyl radical, the H atom-abstractions from position 3 and 4 were found to be the most important channels below 1270 K, while the formation of MLR1 starts dominating above. Total rate constants for the two different H atom-abstraction reactions are shown as Arrhenius plots in Fig. 3 and 4. Temperature dependent branching ratio for the H-abstraction reactions by OH is presented in Fig. 5. Moreover, from the rate expressions of the OH reactions, the total rate constant at 298 K was derived yielding a value of 1.32×10^{12} cm^3 mol^{-1} s^{-1}. In order to validate our results, we estimated the rate constant equal to 1.22×10^{12} cm^3 mol^{-1} s^{-1} using the structure–activity relationship[37] (SAR). The comparison shows a very good agreement between SAR and our computations.

At this point, it should be denoted that the IRC calculations regarding the OH reactions, revealed the possible existence of several pre-reaction and post-reaction complexes. Therefore for these cases, with input structures the end-point structures obtained from the reverse and forward IRC calculations, geometry optimization and vibrational frequency calculations were conducted at the MP2/aug-cc-pVDZ level of theory. These calculations verified and demonstrated the optimized structures of the pre-reaction and post-reaction complexes. Moreover, for these structures single-point energy calculations were performed as previously with the G3 theory. Consequently, the relative zero-point corrected potential energy diagrams were designed. Some representative diagrams are presented in Fig. 6–8. In addition, in the case of the OH abstraction yielding MLR6, no formation of complex was observed. Finally, the presence of these complexes would affect the kinetics of these reactions, at temperatures lower than those considered in the present study. Interestingly, as can be seen from Fig. 7 and 8, the pre-reaction complexes are almost identical in terms of both structure and energy. It seems that the particular interaction at this site of methyl levulinate facilitates the abstraction of the two adjacent hydrogen atoms at C3 and C4 carbon sites, respectively.

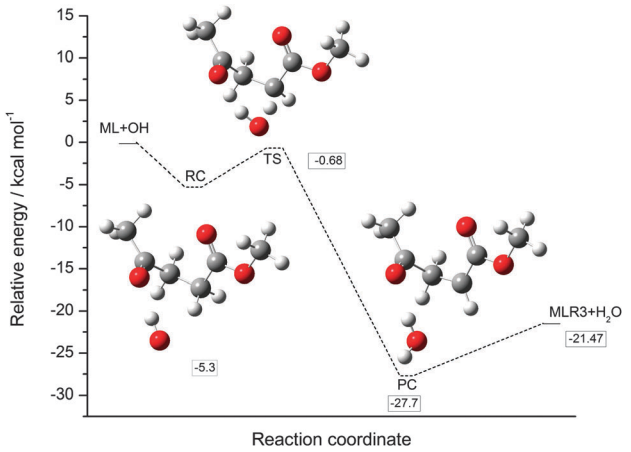

Fig. 7 Relative zero-point corrected potential energy diagram for the reaction ML + OH yielding MLR3 obtained from G3//MP2/aug-cc-pVDZ calculations. RC: pre-reaction complex, TS: transition state, PC: post-reaction complex.

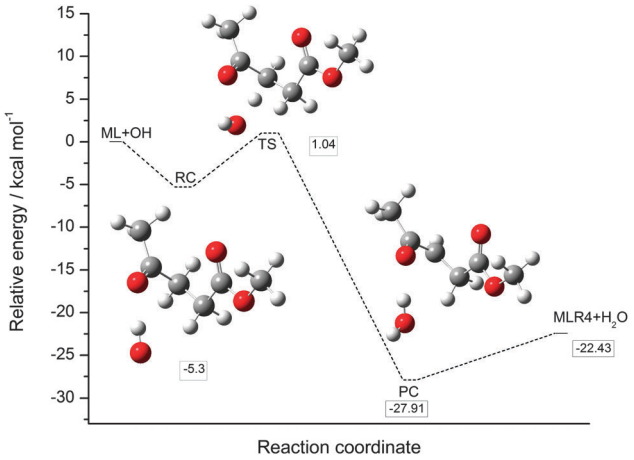

Fig. 8 Relative zero-point corrected potential energy diagram for the reaction ML + OH yielding MLR4 obtained from G3//MP2/aug-cc-pVDZ calculations. RC: pre-reaction complex, TS: transition state, PC: post-reaction complex.

Table 3 Calculated enthalpies of formation for methyl levulinate radicals based on the G3//MP2/aug-cc-pVDZ level of theory

Methodology	MLRN radical	$\Delta_f H^0_{298.15K}$ (kcal mol^{-1})
Atomization scheme (reaction scheme)	MLR1	−95.3 (−94.4)
	MLR3	−98.3 (−97.4)
	MLR4	−99.1 (−98.3)
	MLR6	−97.8 (−96.9)

(b) Unimolecular reactions of radicals deriving from ML oxidation

Unimolecular decomposition reactions of the four radicals produced were investigated. In this section, isomerization as well as beta scission reactions were considered (see Fig. 2). Before the kinetic results will be presented in four different sections for each of the four radicals produced by the initial oxidation, the standard enthalpy of formation of the four radicals was evaluated by means of the atomization scheme as well as by the following reaction scheme (N = 1, 3, 4, 6) (Table 3):

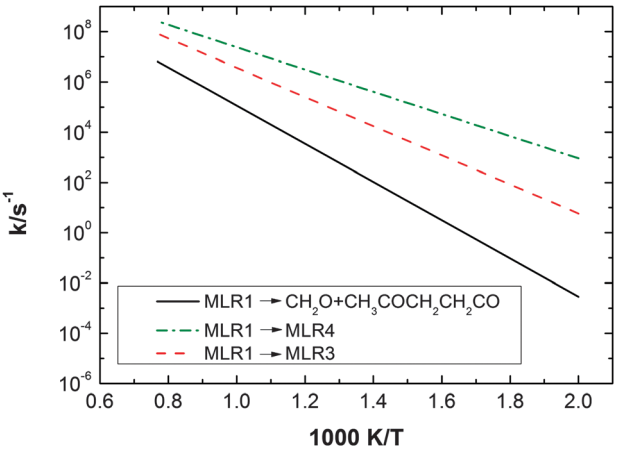

Fig. 9 Arrhenius plot of the unimolecular rate constants for the MLR1 radical.

$$\mathrm{ML} \rightarrow \mathrm{MLRN} + \mathrm{H}$$

Regarding this reaction scheme, the standard enthalpy of formation used for methyl levulinate was the average value calculated (Section 3), whereas for the hydrogen atom we used the proposed experimental value equal to 52.1 kcal mol^{-1}.[38]

(i) MLR1 reactions. Three different reaction pathways of the ((4-oxopentanoyl)oxy)methyl radical (MLR1) were identified and their unimolecular rate constants were characterized. These reactions involve the 1,4-H-shift of MLR1 to MLR3 and 1,5-H-shift resulted in MLR4 as well as the beta scission reaction of MLR1 yielding formaldehyde (CH_2O) and the 4-oxopentanoyl radical ($CH_3COCH_2CH_2CO$). The corresponding rate constants are shown in Fig. 9 and their modified Arrhenius parameters are tabulated in Table 4. It is clearly seen from the Arrhenius plot that the 1,5-H-shift to MLR4 is the major channel over the whole temperature range studied, followed by the 1,4-H-shift reaction to MLR3. The beta scission rate constant is at least one order of magnitude lower than that of the 1,5-H-shift to MLR4, even at high temperatures.

(ii) MLR3 reactions. For the MLR3 radical four different pathways were found and their kinetics were determined. The reactions for the isomerization to MLR1 and MLR6, the beta scission reactions producing methyl acrylate ($CH_3OCOCHCH_2$, MAC) and the acetyl radical (CH_3CO) as well as pent-1-ene-1,4-dione (CH_3COCH_2CHCO) and the methoxy radical (CH_3O),

Table 4 Unimolecular rate constants for the MLR1 radical

Reaction	A (s^{-1})	n	E_a (kcal mol^{-1})
MLR1 → CH_2O + $CH_3COCH_2CH_2CO$	1.14×10^{13}	−0.12	34.94
MLR1 → MLR4	1.75×10^{11}	0.17	20.00
MLR1 → MLR3	2.56×10^{11}	0.29	26.13

Table 5 Unimolecular rate constants for the MLR3 radical

Reaction	A (s^{-1})	n	E_a (kcal mol^{-1})
MLR3 → $CH_3OCOCHCH_2$ + CH_3CO	6.78×10^{12}	0.22	23.77
MLR3 → CH_3O + CH_3COCH_2CHCO	8.45×10^{11}	0.51	48.62
MLR3 → MLR1	4.13×10^{10}	0.60	28.03
MLR3 → MLR6	3.54×10^{10}	0.54	23.37

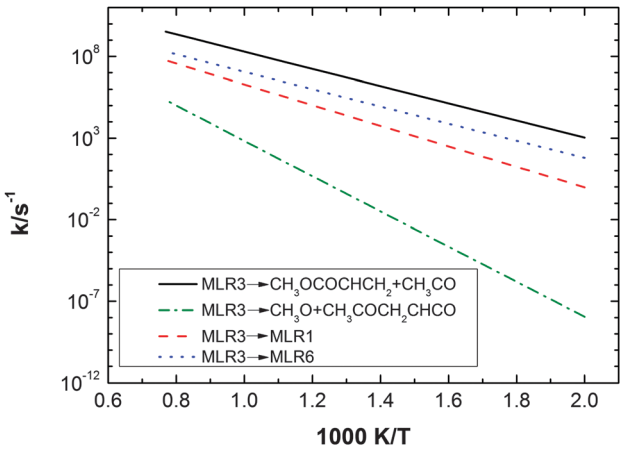

Fig. 10 Arrhenius plot of the unimolecular rate constants for the MLR3 radical.

respectively. Their Arrhenius parameters are given in Table 5. The rate constant for the formation of methyl acrylate and the acetyl radical was found to be the largest amongst the unimolecular rate constants (Fig. 10).

(iii) MLR4 reactions. For 1-methoxy-1,4-dioxopentan-3-yl (MLR4) radical three different reaction pathways were identified

Table 6 Unimolecular rate constants for the MLR4 radical decomposition

Reaction	A (s^{-1})	n	E_a (kcal mol^{-1})
MLR4 → CH_3OCO + $C_2H_3COCH_3$	4.29×10^{12}	0.30	35.45
MLR4 → CH_3 + CH_3OCOCH_2CHCO	8.15×10^{12}	0.30	41.50
MLR4 → MLR1	4.22×10^{9}	0.52	22.59

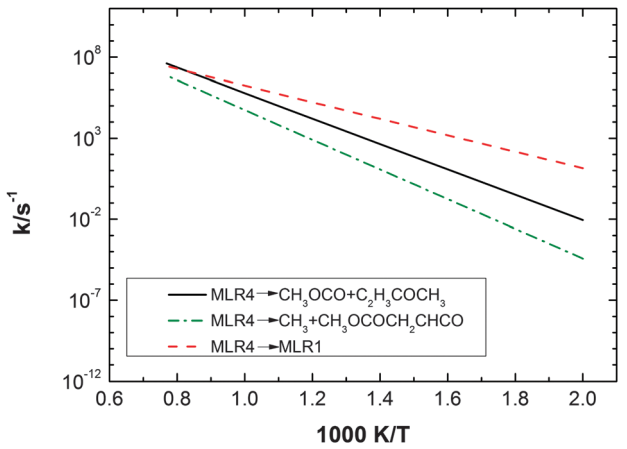

Fig. 11 Arrhenius plot of the unimolecular rate constants for the MLR4 radical.

Table 7 Unimolecular rate constants for the MLR6 radical

Reaction	A (s^{-1})	n	E_a (kcal mol^{-1})
MLR6 → CH_2CO + $CH_3OCOCH_2CH_2$	3.50×10^{11}	0.58	35.20
MLR6 → MLR3	4.39×10^{10}	0.58	22.31

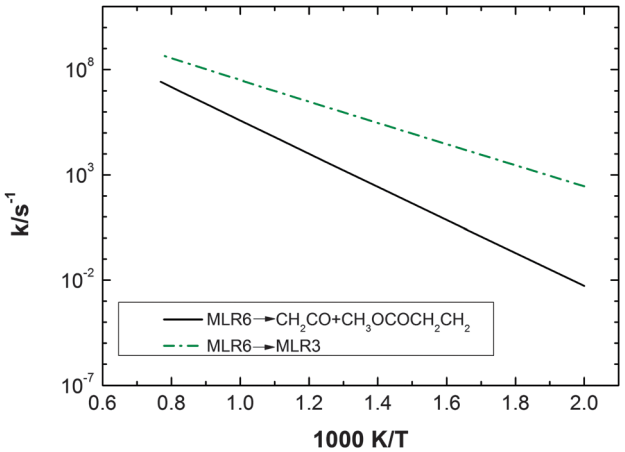

Fig. 12 Arrhenius plot of the unimolecular rate constants for the MLR6 radical.

and their kinetics was computed. These reactions involve the 1,5-H-shift to MLR1, the beta scission reactions yielding methyl-vinyl-ketone ($C_2H_3COCH_3$, MVK) and methoxycarbonyl radical (CH_3OCO), and methyl 4-oxobut-3-enoate (CH_3OCOCH_2CHCO) and the methyl radical (CH_3), respectively. At high temperature, these channels compete with each other, while 1,5-H-shift dominates over the lower temperature range ($T < 1206$ K) (Table 6 and Fig. 11).

(iv) MLR6 reactions. The MLR6 radical can undergo two different reaction pathways with significant rate constants in the temperature range of our interest, namely the 1,4-H-shift to MLR3 and the beta scission reaction producing ketene (CH_2CO) and the 3-methoxy-3-oxopropyl radical ($CH_3OCOCH_2CH_2$). Amongst these channels, the isomerization is the major channel over the temperature range studied (Table 7 and Fig. 12).

Conclusions

The oxidation of methyl levulinate was studied at the G3//MP2/aug-cc-pVDZ level of theory. Rate constants for H-abstraction reactions by hydroxyl and methyl radicals were computed using Transition State Theory (TST) for temperatures ranging from 500 to 1300 K. As expected, rate constants obtained for the OH radical are faster than that of CH_3 radical and the formation of the 1-methoxy-1,4-dioxopentan-3-yl (MLR4) radical is the kinetically more favorable. Pre-reaction and post-reaction complexes were also identified for the reactions of the fuel with the OH radical leading to MLR1, MLR3 and MLR4. These complexes are negligible for kinetic purpose under combustion conditions (high temperatures), but they may affect the kinetics of these reactions at lower temperatures ($T < 400$ K). The total abstraction rate constant for OH (298 K) was derived yielding a value of

1.32×10^{12} cm^3 mol^{-1} s^{-1}. This value reveals a very good agreement with the SAR estimated rate constant (1.22×10^{12} cm^3 mol^{-1} s^{-1}).

The fate of the fuel radicals was then investigated by considering two types of reactions: beta-scission and H atom-transfer reactions. The fastest decomposition reactions for MLR1 and MLR6 radicals are their conversion to MLR3 or MLR4 which will in turn decompose to methyl acrylate (MAC) and methyl vinyl ketone (MVK), respectively. These two compounds are expected to be the main oxidation products of methyl levulinate oxidation, which is also supported by preliminary results of our experiments.

Thermodynamic data (namely enthalpies of formation, heat of combustion, constant pressure heat capacities and entropies at 298 K) were also computed for the fuel and its radicals using different schemes and methods. The maximum deviation between these different strategies was found to be less than 1 kcal mol^{-1}, which gives confidence regarding the accuracy of the present results. The data presented here can be used as a basis for the development of a methyl levulinate oxidation mechanism.

Acknowledgements

The research leading to these results has received funding from the European Research Council under the European Community's Seventh Framework Programme (FP7/2007–2013)/ERC grant agreement No. 291049 – 2G-CSafe. The authors would like to thank László Müller and Máté Labádi for the administration of the computing systems used for this work. Milán Szőri was a Magyary Zoltán Fellow supported by State of Hungary and the European Union, financed by the European Social Fund in the framework of TÁMOP 4.2.4.A/2-11-1-2012-0001 ''National Excellence Program'' under the respective grant number of A2-MZPD-12-0139. This paper was supported by the János Bolyai Research Scholarship of the Hungarian Academy of Sciences (BO/00113/15/7).

Notes and references

1 J. Han, G. S. Forman, A. Elgowainy, H. Cai, M. Wang and V. B. DiVita, *Fuel*, 2015, **157**, 292–298.
2 D. E. Resasco, S. Sitthisa, J. Faria, T. Prasomsri and M. P. Ruiz, in *Heterogeneous Catalysis in Biomass to Chemicals and Fuels*, ed. D. Kubička and I. Kubičková, Research Signpost, 2011.
3 V. Menon and M. Rao, *Prog. Energy Combust. Sci.*, 2012, **38**, 522–550.
4 B. Joffres, D. Laurenti, N. Charon, A. Daudin, A. Quignard and C. Geantet, *Oil Gas Sci. Technol.*, 2013, **68**, 753–763.
5 J.-P. Lange, E. Van Der Heide, J. Van Buijtenen and R. Price, *ChemSusChem*, 2012, **5**, 150–166.
6 J. J. Bozell, L. Moens, D. C. Elliott, Y. Wang, G. G. Neuenscwander, S. W. Fitzpatrick, R. J. Bilski and J. L. Jarnefeld, *Resour., Conserv. Recycl.*, 2000, **28**, 227–239.
7 J. J. Bozell and G. R. Petersen, *Green Chem.*, 2010, **12**, 539–554.
8 M. J. Climent, A. Corma and S. Iborra, *Green Chem.*, 2014, **16**, 516–547.
9 A. Démolis, N. Essayem and F. Rataboul, *ACS Sustainable Chem. Eng.*, 2014, **2**, 1338–1352.
10 *Netherlands Pat.*, WO2004035713, 2004.
11 *Netherlands Pat.*, WO20050016058, 2005.
12 *Netherlands Pat.*, WO2005044960, 2005.
13 *Great Britain Pat.*, GB2478137A, 2011.
14 *Israel Pat.*, WO2010106536, 2010.
15 *Great Britain Pat.*, WO2003002696, 2003.
16 *Germany Pat.*, WO9421753, 1994.
17 *US Pat.*, US20100313467, 2010.
18 E. Christensen, A. Williams, S. Paul, S. Burton and R. L. McCormick, *Energy Fuels*, 2011, **25**, 5422–5428.
19 A. Janssen, S. Pischinger and M. Muether, *SAE Int. J. Fuels Lubr.*, 2010, **3**, 70–84.
20 Molecular Operating Environment (MOE), 2013.08; Chemical Computing Group Inc., 1010 Sherbooke St. West, Suite #910, Montreal, QC, Canada, H3A 2R7, 2015.
21 M. J. Frisch, G. W. Trucks, H. B. Schlegel, G. E. Scuseria, M. A. Robb, J. R. Cheeseman, G. Scalmani, V. Barone, B. Mennucci, G. A. Petersson, H. Nakatsuji, M. Caricato, X. Li, H. P. Hratchian, A. F. Izmaylov, J. Bloino, G. Zheng, J. L. Sonnenberg, M. Hada, M. Ehara, K. Toyota, R. Fukuda, J. Hasegawa, M. Ishida, T. Nakajima, Y. Honda, O. Kitao, H. Nakai, T. Vreven, J. A. Montgomery, Jr., J. E. Peralta, F. Ogliaro, M. Bearpark, J. J. Heyd, E. Brothers, K. N. Kudin, V. N. Staroverov, R. Kobayashi, J. Normand, K. Raghavachari, A. Rendell, J. C. Burant, S. S. Iyengar, J. Tomasi, M. Cossi, N. Rega, N. J. Millam, M. Klene, J. E. Knox, J. B. Cross, V. Bakken, C. Adamo, J. Jaramillo, R. Gomperts, R. E. Stratmann, O. Yazyev, A. J. Austin, R. Cammi, C. Pomelli, J. W. Ochterski, R. L. Martin, K. Morokuma, V. G. Zakrzewski, G. A. Voth, P. Salvador, J. J. Dannenberg, S. Dapprich, A. D. Daniels, Ö. Farkas, J. B. Foresman, J. V. Ortiz, J. Cioslowski and D. J. Fox, *Gaussian 09, Revision D.01*, Wallingford CT, 2009.
22 E. P. Faragó, M. Szőri, M. C. Owen, C. Fittschen and B. Viskolcz, *J. Chem. Phys.*, 2015, **142**, 054308.
23 M. Szori, C. Fittschen, I. G. Csizmadia and B. Viskolcz, *J. Chem. Theory Comput.*, 2006, **2**, 1575–1586.
24 C. Bänsch, J. Kiecherer, M. Szöri and M. Olzmann, *J. Phys. Chem. A*, 2013, **117**, 8343–8351.
25 C. Møller and M. S. Plesset, *Phys. Rev.*, 1934, **46**, 618–622.
26 R. A. Kendall, T. H. Dunning and R. J. Harrison, *J. Chem. Phys.*, 1992, **96**, 6796–6806.
27 A. G. Baboul, L. A. Curtiss, P. C. Redfern and K. Raghavachari, *J. Chem. Phys.*, 1999, **110**, 7650–7657.
28 J. M. Simmie and K. P. Somers, *J. Phys. Chem. A*, 2015, **119**, 7235–7246.
29 NIST Computational Chemistry Comparison and Benchmark Database, http://cccbdb.nist.gov/.
30 R. Dennington, T. Keith and J. Millam, *GaussView, Version 5*, Semichem Inc., Shawnee Mission, KS, 2009.

31 S. Canneaux, F. Bohr and E. Henon, *J. Comput. Chem.*, 2014, **35**, 82–93.
32 G. Herzberg, *Molecular Spectra and Molecular Structure, Vol. I: Spectra of Diatomic Molecules*, Krieger, Malabar, FL, 2nd edn, 1989.
33 J. A. Montgomery, M. J. Frisch, J. W. Ochterski and G. A. Petersson, *J. Chem. Phys.*, 1999, **110**, 2822–2827.
34 M. A. V. Ribeiro daSilva, M. L. C. C. H. Ferrao and F. Jiye, *J. Chem. Eng. Data*, 1995, **40**, 426–428.
35 *CRC Handbook of Chemistry and Physics*, CRC Press/Taylor and Francis, Boca Raton, FL, 89th edn (Internet Version 2009) 2009, 8129673.
36 S. Sharma, M. R. Harper and W. H. Green, *Combust. Flame*, 2010, **157**, 1331–1345.
37 E. S. C. Kwok and R. Atkinson, *Atmos. Environ.*, 1995, **29**, 1685–1695.
38 B. Ruscic, R. E. Pinzon, M. L. Morton, G. von Laszevski, S. J. Bittner, S. G. Nijsure, K. A. Amin, M. Minkoff and A. F. Wagner, *J. Phys. Chem. A*, 2004, **108**, 9979–9997.